Neurobiology of Disease

Familial Alzheimer's Disease Presenilin 1 Mutations Cause Alterations in the Conformation of Presenilin and Interactions with Amyloid Precursor Protein

Oksana Berezovska, Alberto Lleo, Lauren D. Herl, Matthew P. Frosch, Edward A. Stern, Brian J. Bacskai, and Bradley T. Hyman

Alzheimer Research Unit, Massachusetts General Hospital, Charlestown, Massachusetts 02129

Presenilin 1 (PS1) is a critical component of the γ-secretase complex, an enzymatic activity that cleaves amyloid β (Aβ) from the amyloid precursor protein (APP). More than 100 mutations spread throughout the PS1 molecule are linked to autosomal dominant familial Alzheimer's disease (FAD). All of these mutations lead to a similar phenotype: an increased ratio of $Aβ_{42}$ to $Aβ_{40}$, increased plaque deposition, and early age of onset. We use a recently developed microscopy approach, fluorescence lifetime imaging microscopy, to monitor the relative molecular distance between PS1 N and C termini in intact cells. We show that FAD-linked missense mutations located near the N and C termini, in the mid-region of PS1, and the exon 9 deletion mutation all change the spatial relationship between PS1 N and C termini in a similar way, increasing proximity of the two epitopes. This effect is opposite of that observed by treatment with $Aβ_{42}$-lowering nonsteroidal anti-inflammatory drugs (NSAIDs) (Lleo et al., 2004b). Accordingly, treatment of M146L PS1-overexpressing neurons with high-dose NSAIDs somewhat offsets the conformational change associated with the mutation. Moreover, by monitoring the relative distance between a PS1 loop epitope and the APP C terminus, we demonstrate that the FAD PS1 mutations are also associated with a consistent change in the configuration of the PS1–APP complex. The nonpathogenic E318G PS1 polymorphism had no effect on PS1 N terminus–C terminus proximity or PS1–APP interactions. We propose that the conformational change we observed may therefore provide a shared molecular mechanism for FAD pathogenesis caused by a wide range of PS1 mutations.

Key words: **fluorescence lifetime imaging microscopy (FLIM); presenilin 1; amyloid precursor protein; amyloid β peptide; familial Alzheimer's disease; γ-secretase**

Introduction

Deposition of amyloid β (Aβ)-containing plaques in the brain is one of the major neuropathological hallmarks of Alzheimer's disease (AD). The final enzymatic step in generating Aβ via intramembranous cleavage of amyloid precursor protein (APP) is performed by the presenilin 1 (PS1)-dependent γ-secretase complex (Fraser et al., 2000; Selkoe, 2001; Fortini, 2002). PS1 is a 467 aa eight-transmembrane domain (TM) protein with proposed N and C termini and a major loop domain (between predicted TM6 and TM7) oriented toward the cytoplasm (Doan et al., 1996; Li and Greenwald, 1996, 1998). During maturation, PS1 associates with a high-molecular weight complex and undergoes proteolysis within exon 9, yielding a stable functionally active heterodimeric complex of N- and C-terminal fragments (Thinakaran et al., 1996; Podlisny et al., 1997; Seeger et al., 1997; Capell et al., 1998; Yu et al., 1998; Levitan et al., 2001). The immature PS1 holoprotein (or PS1 that does not undergo proteolysis because of mutated aspartates in TM6 or TM7) (Wolfe et al., 1999) does not support γ-secretase activity. Thus, to become functionally active, PS1 must undergo posttranslational modification and associate within the membrane with at least three other transmembrane proteins: nicastrin, aph-1, and pen-2 (Yu et al., 2000; Francis et al., 2002; Goutte et al., 2002). Because of these complexities, efforts at direct structural analysis of the members of the γ-secretase complex have not yet been successful.

More than 100 autosomal dominantly inherited familial AD (FAD) mutations have been found in PS1, widely scattered from the N terminus (NT) to the C terminus (CT) (Selkoe, 2001). We hypothesized that because the widely spaced FAD PS1 mutations nearly universally lead to a similar biochemical, histological, and clinical phenotype, they may cause similar molecular alterations in PS1. To examine the subdomain structure of PS1 *in situ* in intact cells, we used a recently developed fluorescence resonance energy transfer (FRET) microscopy approach, fluorescence lifetime imaging microscopy (FLIM) (Lleo et al., 2004b). A FRET signal is observed only if two fluorophores are less than ~5–10 nm from one another; even if the fluorophores decorate two

Received Aug. 26, 2004; revised Jan. 31, 2005; accepted Feb. 1, 2005.

This work was supported by National Institutes of Health Grants P01 AG15379-06 and EB00768 (B.J.B.), a Paul Beeson Physician Faculty Scholar in Aging Research Award (M.P.F.), a Pioneer Award from the Alzheimer Association (B.T.H.), and by the Walters Family Foundation. We thank Dr. D. Selkoe for stably transfected CHO cell lines and for x81 and C8 antibodies and Drs. C. Haass and T. Golde for PS1 mutant PS1 plasmids (L166P and G384A; and M139V, respectively).

Correspondence should be addressed to either of the following: Dr. Oksana Berezovska, Alzheimer Research Unit, Room 2750, Massachusetts General Hospital, 114 Sixteenth Street, Charlestown, MA 02129, E-mail: oberezovska@partners.org; or Dr. Bradley Hyman, Alzheimer Research Unit, Room 2009, Massachusetts General Hospital, 114 Sixteenth Street, Charlestown, MA 02129, E-mail: bhyman@partners.org.

DOI:10.1523/JNEUROSCI.0364-05.2005

 0270-6474/05/253009-09$15.00/0

Table 1. Proximity between various epitopes in the wild-type PS1 molecule

FRET donor (FITC labeled)	FRET acceptor (Cy3 labeled)	FITC lifetime (mean ± SD)	*p* value (compared with FITC)
PS1 NT ($n = 13$)	None	2405 ± 90 ps	–
PS1 NT ($n = 12$)	GRP78/BiP	2325 ± 91 ps	ns
PS1 CT ($n = 13$)	PS1 loop	1748 ± 258 ps	<0.001
PS1 NT ($n = 20$)	PS1 CT	1674 ± 394 ps	<0.001

Time-domain FLIM and a biexponential decay curve fitting were used to calculate average FITC lifetimes ($t1$ and $t2$) in each cell. First, FITC lifetime ($t1$) in the absence of FRET (in PS1 NT–BiP double-immunostained cells; negative control) was calculated using FLIM software. To analyze proximity between different epitopes of the PS1 molecule, the average FITC lifetimes per cell were fitted to two curves representing the non-FRETing population (fixed as $t1$) and a second population ($t2$). A shorter lifetime ($t2$) implies the presence of FRET and a close proximity (<10 nm) between the donor and acceptor. In the absence of FRET (the donor and acceptor fluorophores are far apart), $t2$ is not significantly different from $t1$. One-way ANOVA was performed to analyze differences in the lifetime, followed by least significant difference *post hoc* analysis. Levene's test was also performed to determine whether variances were equal. ns, Not significant; *n*, cell number.

epitopes of a single protein, the presence and amount of FRET can vary substantially depending on the exact spatial relationship of the donor and acceptor fluorophore. We have recently shown, using this FLIM technique (Lleo et al., 2004b), that the proximity of the PS1 NT to the PS1 CT and of the PS1 loop to the APP CT, are altered by nonsteroidal anti-inflammatory drugs (NSAIDs) that lower $A\beta_{42}$ (Weggen et al., 2001). We have now applied this FLIM technique to evaluate whether the conformation of functionally active PS1 heterodimer differs from that of inactive PS1 holoprotein and to elucidate how PS1 mutations affect the spatial relationship between N and C termini of the PS1 molecule. An analogous assay was also used to determine how FAD-linked changes in PS1 alter its interactions with APP.

Materials and Methods

Cells and transfections. Primary neurons were prepared as described previously (Berezovska et al., 1999). Briefly, transgenic mice heterozygous for human wild-type or M146L mutant PS1 were used (at embryonic day 16) to prepare primary neuronal cultures from the cortex and hippocampus. Neurons were maintained in chemically defined Neurobasal medium (Invitrogen, Gaithersburg, MD) containing 2% B27 supplement (Invitrogen). After 4–14 d *in vitro*, the cells were immunostained for the FLIM analysis.

Chinese hamster ovary (CHO) cells stably expressing wild-type APP and N2a mouse neuroblastoma cells were used for transient transfections of wild-type and FAD mutant PS1. Superfect reagent (Qiagen, Valencia, CA) was used for transient transfections according to the manufacturer's instructions. Alternatively, CHO cells stably expressing wild-type APP and wild-type PS1, aspartate mutant, or FAD mutant PS1 were examined (gifts from Dr. D. Selkoe, Brigham and Women's Hospital, Boston, MA).

To analyze whether RNA interference (RNAi)-mediated knockdown of nicastrin (Nct) affects normal PS1 conformation, we used 21-mer double-stranded RNAi (Dharmacon Research, Lafayette, CO) directed against Nct (Edbauer et al., 2002) to transfect cells (Effectene reagents; Qiagen). Mock transfected cells (nonsense primer) served as a control (Berezovska et al., 2003).

NSAID treatment. Cultures of primary neurons from the wild-type PS1 or M146L PS1 transgenic mice were treated with ibuprofen (375 μM), indomethacin (150 μM), or 0.3% ethanol (EtOH; vehicle control) for 24 h before fixation and FLIM analysis.

Antibodies and immunocytochemistry procedures. For the analysis of PS1 conformation, cells were double-immunostained with antibodies against the PS1 NT [goat α-human PS1 directed against amino acids 14–33 (Sigma, St. Louis, MO) or 81× directed against amino acids 1–81 (kindly provided by Dr. Selkoe)] and against the PS1 CT [rabbit α-human S182 antibody (amino acids 450–467; Sigma) or C-20 antibody (Santa Cruz Biotechnology, Santa Cruz, CA). For the analysis of PS1–APP interactions, the cells were immunostained with an antibody against the APP CT [C8 antibody raised against amino acids 676–695 of APP (Selkoe et al., 1988)] and an antibody to the major loop between PS1 TM6 and TM7 (mouse αPS1, amino acids 263–378; Chemicon, Temecula, CA). Pairs of primary antibodies were labeled with secondary antibodies conjugated to FITC or cyanine 3 (Cy3) for the FLIM analysis.

FLIM assay. The cells were fixed and double-immunostained for the FLIM analysis as described previously (Berezovska et al., 2003; Lleo et al., 2004b). Briefly, fluorescence lifetime of a donor fluorophore (FITC) was measured if the FRET acceptor fluorophore (Cy3) was absent or was >10 nm away from the FITC donor (negative control). If the two fluorophores are <5–10 nm apart, FRET occurs and the donor fluorophore lifetime shortens. In each experiment, negative controls consisted of cells immunostained with donor fluorophore only or double-immunostained with antibodies against antigens known not to interact (no FRET present), such as GRP78/BiP (StressGen Biotechnologies, Victoria, British Columbia, Canada) and PS1 (see Fig. 1*A*,*B*). Positive controls included Cy3–anti-mouse IgG/FITC-immunostained cells (Berezovska et al., 2003). The FLIM software uses the Levenberg–Marquardt algorithm to fit the raw data from each pixel to multi-exponential fluorescence decay curves to calculate FITC fluorescence lifetimes with the following formula: $t = a_1e^{-t/\tau 1} + a_2e^{-t/\tau 2} + a_3e^{-t/\tau 3} + a_ne^{-t/\tau n}$, where t is the fluorescence lifetime of the donor fluorophore (FITC) measured in picoseconds after a short (100 fs) pulse of excitation light, and τ is the time at which the fluorescence decays to $1/e$ of the initial value. With complex decay times, the curves are fit with multiple exponentials by using multiple τ. Each exponential component has a weighted amplitude (a_1, a_2, . . . a_n) that is expressed as a percentage of the sum of the amplitudes from each component. For a single-exponential fit, $a1 = 100\%$. To represent a "non-FRETing" population with a longer lifetime ($t1$) and a "FRETing" population with a shorter lifetime ($t2$), the fluorescence lifetimes are fitted to two curves. The $t2$ values are presented in Tables 1–5. In the negative control, the non-FRETing population contains all of the fluorophores and does not have a shorter lifetime (i.e., $t1 = t2$).

A femtosecond-pulsed Ti:Sapphire laser (Mai-Tai; Spectra-Physics, Mountain View, CA) at 800 nm coupled with a Radiance 2000 microscope (Bio-Rad, Hercules, CA) was used for multiphoton fluorescence excitation. FITC fluorescence was acquired using an emission filter centered at 515/30 nm. Fluorescence lifetimes were recorded using a high-speed photomultiplier tube with a full-width half-maximal response time of ~50 ps (MCP R3809; Hamamatsu, Hamamatsu City, Japan) and a fast time-correlated single-photon counting acquisition board (SPC-830; Becker & Hickl, Berlin, Germany) that allows high temporal resolution lifetime acquisition with high spatial resolution imaging (Bacskai et al., 2003). A 128 × 128 pixel matrix was created with the single-exponential (for FITC alone) or multi-exponential (for FITC and Cy3 double-immunostained cells) curve fit data for each pixel, allowing color-coding by lifetime.

Results

Establishment of a PS1 subdomain conformation assay

Our previous studies suggested that antibodies directed against the NT and the CT of PS1 were in close enough proximity to support FRET and therefore would be one read-out of PS1/γ secretase conformation (Lleo et al., 2004b). To confirm and extend these analyses, CHO cells stably expressing wild-type PS1 were double-immunostained with the following pairs of fluorescently labeled antibodies: against the NT and CT or against a major loop between TM6 and TM7 (loop) and the CT of the PS1 molecule. The relative proximity between these PS1 epitopes was evaluated by measuring lifetimes of the FITC donor fluorophore (Table 1). The extent of shortening of the fluorescence lifetime reflects the distance between the two labeled epitopes. When

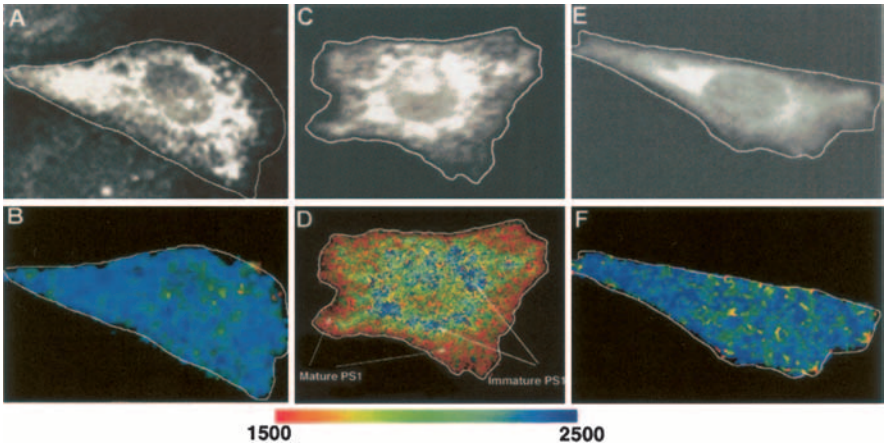

Figure 1. FLIM analysis of the subcellular distribution of the PS1 holoprotein and heteroprotein populations. ***A***, ***B***, Negative control. CHO cells double-immunostained with antibodies to the PS1 NT (***A***, intensity image) and to ER resident BiP are shown. ***B***, The FLIM image shows pseudocolored PS1–FITC lifetime, which is ~ 2300 ps. ***C***, ***E***, Intensity image of the FITC–PS1 immunostaining in the wild-type PS1 (***C***)- and D257A PS1 (***E***)-expressing CHO cell. ***D***, ***F***, Color-coded FLIM images of the FITC lifetimes in the cell shown in ***C*** and ***E***, respectively. The continuous colorimetric scale shows color-coded fluorescence lifetime in picoseconds. A shorter lifetime represents closer proximity between the fluorophore-labeled PS1 NT and CT and is shown in red. Absence of FRET between the fluorophores on PS1 N and C termini results in a longer FITC lifetime and is indicated in blue. The cell profiles are shown by tracings.

FRET occurs, we observe a population with a statistically shorter lifetime (less than ~2000 ps). As negative controls, we examined lifetimes of PS1 FITC stained without an acceptor (Cy3) present, or PS1 FITC stained with an acceptor present on GRP78-BiP, which colocalizes with PS1 in the endoplasmic reticulum but is too distant to support FRET. In both instances, only non-FRETing FITC lifetimes of ~2300–2400 ps were observed.

As expected, all pairs of PS1 antibodies showed complete colocalization at the light microscopic (confocal) level (Fig. 1*C*, intensity image). Two sets of pairs were in close enough proximity to support FRET (Table 1). We observed a shortening of lifetime, consistent with close proximity, between the loop domain fluorophores and the nearby CT fluorophore. We also observed a large change in the FITC lifetime, suggesting close proximity between the N and C termini of the PS1 molecule, confirming our previous observations with an additional pair of antibody reagents (Sigma).

The FLIM software measures fluorescence lifetimes and generates fluorescence decay curves in each pixel of the image to calculate lifetimes. In this case, fluorescence lifetimes in each pixel were fitted to two curves, representing FRETing (NT and CT of the PS1 molecule are in a close proximity) and non-FRETing populations with a longer lifetime. We found that the majority of FRETing PS1 molecules (Fig. 1*D*, red) were localized in the peripheral subcellular compartments, near or at the plasma membrane, whereas the noninteracting/non-FRETing PS1 population (Fig. 1*D*, blue) was prominent in perinuclear areas. We hypothesized that the population of PS1 molecules in distal cell compartments reflected mature forms, whereas the non-FRETing PS1 molecules in the perinuclear region represented the uncleaved holoprotein.

Conformation of the PS1 holoprotein differs from that of the mature heterodimer

To test this hypothesis, we generated cells in which holoprotein predominates. We used two different approaches: (1) cells expressing active site aspartate mutant PS1 (D257A or D385A), which are known to prevent PS1 endoproteolysis and diminish Aβ production and Notch processing (De Strooper et al., 1999; Wolfe et al., 1999; Berezovska et al., 2000); and (2) Nct RNAi treatment, which prevents PS1 heterodimer formation and disrupts γ-secretase function (Edbauer et al., 2002).

In D257A and D385A PS1 cells, we found that the lifetime of FITC (labeling NT) in the presence of the Cy3-labeled CT was uniform throughout the cell and was significantly longer, compared with that in wild-type PS1 cells, despite a nearly identical pattern of PS1 immunoreactivity in the wild-type and aspartate mutant cells (Fig. 1*E*,*F*). The FITC lifetime in PS1 D257A and D385A cells was not statistically different from the lifetime of FITC in the negative control (Table 2), suggesting that the NT–CT interaction detected in the peripheral subcellular compartments for wild-type PS1 is absent in aspartate mutant PS1 [i.e., that the conformation of the aspartate mutant PS1 holoprotein is different from that of the wild-type PS1 heterodimer (despite similar subcellular localization by immunocytochemistry)].

An alternative approach to generating PS1 holoprotein *in situ* is to knock down a PS1-interacting gene, Nct, which is critical for PS1 maturation. To analyze whether RNAi mediated knockdown of Nct function and abolishment of PS1 endoproteolysis also affects PS1 conformation, we transfected cells with 21-mer double-stranded Nct short interfering RNA (Edbauer et al., 2002). Three days after the treatment, cells were fixed and immunostained for the FLIM analysis. Sister cultures harvested for Western blot analysis confirmed previous observations that Nct expression in Nct RNAi-treated cells was reduced by ~90% (Edbauer et al., 2002; Berezovska et al., 2003). Both D257A/D385A mutant PS1 and PS1 in cells subjected to Nct knock-down was predominantly uncleaved holoprotein (Fig. 2). Similar to PS1 aspartate mutant cells, the lifetime of FITC (PS1 NT) in Nct RNAi-treated cells was uniform and significantly longer than that in wild-type PS1-expressing, untreated cells (Table 2). Thus, PS1 molecules, which were prevented from generating heterodimeric forms by either method, did not show a second population with shortened lifetimes, demonstrating an absence of putative close interaction between the NT and CT of PS1 holoprotein. These results suggest that the FRET signal (i.e., the molecules giving rise to lifetimes shorter than the baseline) derived from PS1 molecules in the mature conformation.

FAD PS1 mutations change PS1 conformation

A FAD-linked PS1 mutation that leads to the deletion of exon 9 (PS1 Δex9) prevents endoproteolysis of PS1, yet results in increased Aβ_{42} generation (Borchelt et al., 1996; Steiner et al., 2001). For the analysis of the spatial relationship between PS1 N and C termini in PS1 Δex9 mutants, CHO cells were transiently transfected with either wild-type or Δex9 mutant PS1. As described above, FLIM lifetime decay measurements were fit to two exponential decays, the first (longer) equivalent to the non-FRETing population as observed for inactive PS1 holoprotein and the second (shorter) reflecting the FRETing population. The average fluorescence lifetimes of the second population ($t2$), rep-

Table 2. Differences in the proximity between N and C termini in the PS1 holoprotein and wild-type heterodimer

Condition	FITC lifetime ($t2$; mean ± SD)	p value (compared with $t1$, FITC–IgG, 2321 ± 59)
PS1 wild type ($n = 55$)	1768 ± 141 ps	<0.001
PS1 D257A ($n = 38$)	2450 ± 126 ps	ns
PS1 D385A ($n = 12$)	2389 ± 82 ps	ns
PS1 (Nct RNAi) ($n = 28$)	2199 ± 185 ps	ns

FITC lifetime ($t1$) in the absence of FRET (in PS1 NT–BiP double-immunostained cells; negative control) was calculated using FLIM software. FITC–IgG lifetime ($t1$) was 2321 ± 59 ps. To analyze PS1 NT and CT proximity, the average FITC lifetimes per cell were fitted to two curves representing the non-FRETing (fixed as $t1$) and FRETing ($t2$) populations. These calculated lifetimes were recorded per cell and are summarized. A $t2$ lifetime shorter than $t1$ lifetime implies the presence of FRET and a close proximity between the donor and acceptor. To generate PS1 holoprotein, the cells were transfected with either Nct RNAi 21-mer dsRNA or D257A, or D385A PS1-expressing stable cell lines were used. One-way ANOVA was performed to analyze differences in the lifetime, followed by least significant difference *post hoc* analysis. Levene's test was also performed to determine whether variances were equal. *n*, Cell number; ns, not significant (ANOVA).

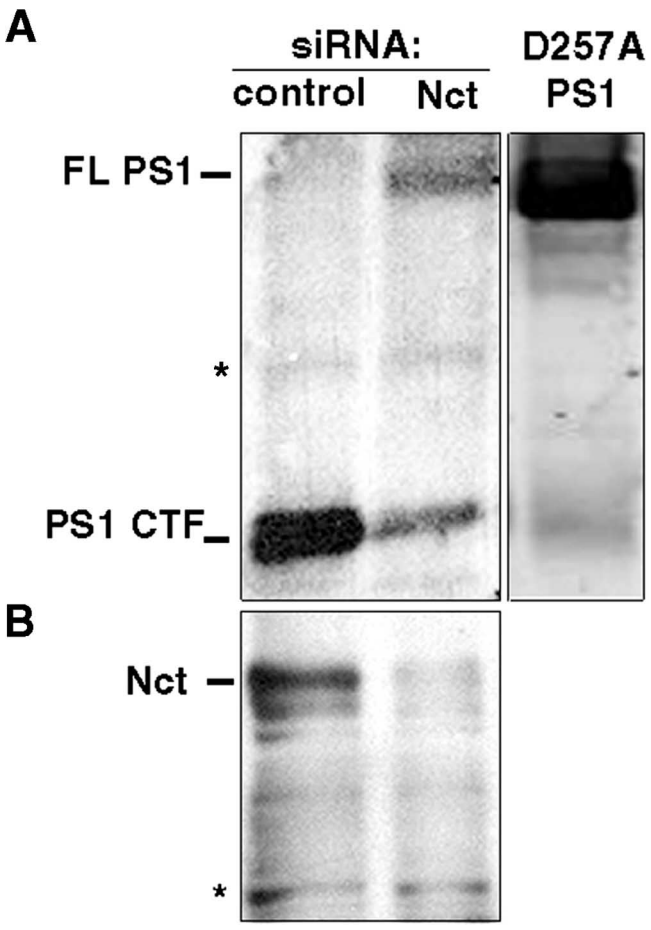

Figure 2. Detection of PS1 and Nct in cells treated with small interfering RNA (siRNA) or in cells expressing aspartate mutant PS1. ***A***, CHO cells were transfected with control or Nct siRNA for 72 h, lysed in a buffer containing 1% Triton X-100, and resolved by electrophoresis on a 4–20% Tris-glycine gel (Invitrogen, Carlsbad, CA). To test the effect of aspartate mutations, we used CHO cells stably expressing D257A mutant PS1. The samples were probed with mouse α-PS1 antibody (Chemicon). PS1 endoproteolysis was significantly reduced in both Nct siRNA- and D257A PS1-transfected cells. ***B***, Nct RNAi-treated cells probed with rabbit α-Nct antibody (Chemicon). The expression of Nct was nearly abolished in Nct siRNA-treated cells. The asterisk indicates nonspecific bands and serves as a loading control. CTF, C-terminal fragment.

resenting the spatial conformation of heterodimeric, catalytically active species were used for all subsequent analyses and are presented in the Tables 1–5. We predicted that the conformation of PS1 Δex9 would be similar to the wild-type active heterodimer, rather than the inactive PS1 holoprotein. Indeed, analysis of PS1

Table 3. Differences in the proximity between N and C termini in wild-type PS1 and FAD mutant PS1

Condition	FITC lifetime ($t2$; mean ± SD; ps)
PS1 wild type ($n = 55$)	1768 ± 141
PS1 Δex9 ($n = 36$)	1019 ± 221*
PS1 M139V ($n = 9$)	1144 ± 54*
PS1 M146L ($n = 36$)	1191 ± 342*
PS1 L166P ($n = 23$)	830 ± 191*
PS1 L286V ($n = 63$)	1054 ± 285*
PS1 G384A ($n = 30$)	849 ± 124*
PS1 C410Y ($n = 37$)	1162 ± 404*
PS1 E318G ($n = 25$)	1817 ± 202

For the analysis of the effect of FAD PS1 mutations, CHO cells were transiently transfected with either wild-type PS1 or FAD mutant PS1. *n*, Cell number. *$p < 0.01$ compared with wild-type PS1 (ANOVA).

Δex9-expressing cells revealed FRET between the N and C termini of PS1 in distal cell compartments, consistent with the conformation of the wild-type heterodimer (and unlike the wild-type holoprotein). Interestingly, the degree of FITC lifetime shortening in PS1 Δex9 exceeded that of wild-type PS1 (Table 3). Thus, these data imply that the functional activity of PS1 relies on a close N and C termini interaction that normally depends on heterodimer formation but can be achieved by a mutation that alters the conformation of PS1 and allows functional activity of PS1 as a holoprotein.

We hypothesized that the change in NT–CT proximity of PS1 Δex9 compared with wild-type PS1 may represent a pathogenic conformational change. To test this hypothesis, we transiently transfected CHO cells with wild-type PS1 or each of six FAD PS1 missense mutations located in different domains of the PS1 molecule: M139V and M146L mutations in TM2, L166P mutation in TM3, L286V mutation (in the hydrophilic loop) between TM6 and TM7, G384A mutation in TM7, and C410Y mutation in TM8. All mutations increase the $A\beta_{42}/A\beta_{40}$ ratio and lead to early-onset autosomal dominantly inherited AD (Borchelt et al., 1996; Scheuner et al., 1996). Similar to the PS1 Δex9 mutation, FLIM measurements revealed a dramatic difference in the FRET measures per cell between wild type and each of the FAD PS1 mutants (Table 3) with shorter lifetimes observed for each mutant PS1 reflecting much closer proximity between PS1 N and C termini. This suggests that the orientation of the N and C termini are consistently altered with respect to one another in all tested FAD mutants compared with wild-type PS1. The change in NT–CT proximity caused by FAD PS1 mutations was the opposite of the change observed in the inactive PS1 holoprotein when compared with the wild-type PS1.

Immunostaining of the cells expressing either wild-type PS1 or FAD mutant PS1 did not show any difference in the localization of PS1 immunoreactivity. Similarly, the distribution of PS1 in FLIM images of the cells expressing FAD mutant PS1 were not noticeably different from that of the wild-type PS1: the majority of the PS1 molecules with the closest NT–CT proximity were observed in the cell periphery (Fig. 3), which suggests that FAD PS1 mutations did not have a substantial enough effect on the maturation/trafficking of the PS1 molecules through the secretory pathway to alter their gross subcellular distribution. Interestingly, the distribution of PS1 "conformations" shown in the FLIM image of the Δex9 mutant PS1, which exists in the cell as uncleaved holoprotein, was similar to that of wild-type PS1 and missense mutant PS1 heterodimers. This suggests that achieving close NT–CT proximity conformation for Δex9 PS1 may depend on trafficking and association with the other members of the γ-secretase complex rather than on PS1 endoproteolysis per se.

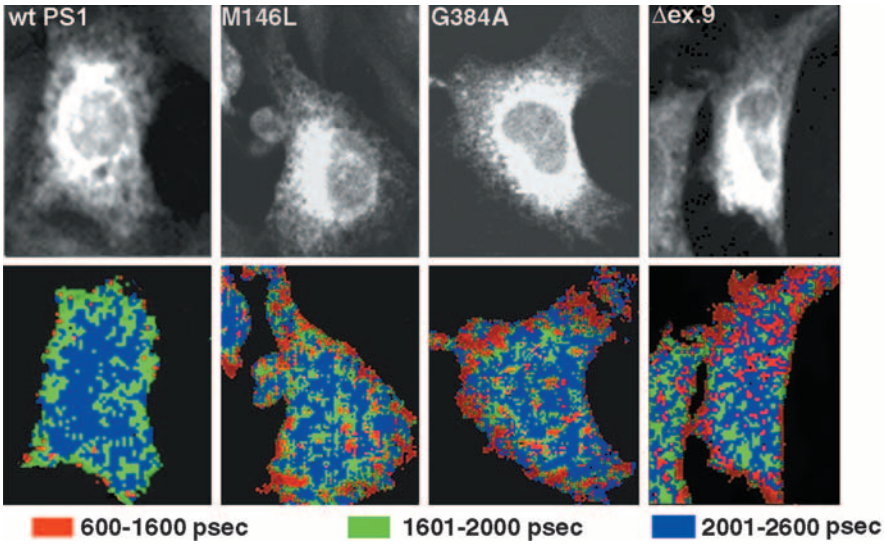

Figure 3. FLIM analysis of the FITC lifetime distribution in CHO cells expressing wild-type (wt) and FAD mutant PS1. The cells were double-immunostained with antibodies against the PS1 NT and CT. The intensity images show the FITC-immunostained N-terminal antibody. Pseudocolored FLIM images show the spatial distribution of the *t*2 FITC–PS1–NT lifetimes in cells expressing wt PS1 and selected representative PS1 mutations: M146L, G384A, and Δex.9. The pseudocolored FLIM images are presented for clarity using discrete colors for fluorescence lifetimes: red, lifetimes between 600 and 1600 picoseconds (psec); green, 1601–2000 psec; blue, 2001–2600 psec. Both red and green denote FRETing populations (shorter FITC lifetime reflects closer PS1 NT–CT proximity), representing functionally active PS1. A population with a majority of non-FRETing PS1 molecules (longer FITC lifetime, PS1 NT–CT far apart) is shown in blue.

To further test whether the decrease in PS1 NT–CT proximity represents a molecular mechanism of the pathogenesis caused by FAD PS1 mutations, we analyzed the effect of a missense polymorphism in PS1 (E318G) that is not associated with AD (Aldudo et al., 1998; Kowalska et al., 2003; Zekanowski et al., 2004). Interestingly, in cells expressing E318G PS1 mutants, FITC–PS1–NT lifetime was significantly different from that of FAD-linked PS1 mutations but not significantly different from wild-type PS1. This suggests that the nonpathogenic E318G polymorphism does not cause the same change in the positioning of the PS1 NT relative to the CT as pathogenic PS1 mutations (Table 3).

Next, we examined whether the observed effects of FAD mutations on PS1 conformation is a result of transient transfection or a cell-type-specific phenomenon. We found that the effect of FAD PS1 mutations on PS1 conformation was similar in CHO and N2a neuroblastoma cells transiently transfected with wild-type PS1 and FAD mutant PS1 plasmids as well as in stably transfected CHO cell lines when wild-type PS1-expressing cells were compared with FAD PS1-expressing cells (data not shown). In addition, all observations were confirmed using two different sets of antibodies to the PS1 NT [x81 (from Dr. Selkoe) and human-specific αNT (Sigma)] and to the PS1 CT [human-specific S182 antibody (Sigma) and C-20 (Santa Cruz Biotechnology)].

Neurons are the main population of cells affected in AD. To further test our findings, we used primary cortical neurons derived from transgenic mice expressing either human wild-type PS1 or M146L PS1 (Berezovska et al., 1999). We found that the average FITC lifetime per cell was significantly shorter in M146L PS1 neurons (1487 ± 108 ps; $n = 36$ neurons) compared with that in wild-type PS1 neurons (1763 ± 204 ps; $n = 45$ neurons; $p < 0.01$; ANOVA). This indicates that the conformation of the mutant PS1 was considerably different from that of the wild-type PS1, with tighter interaction between the PS1 NT and CT in M146L PS1-expressing neurons. There was no noticeable difference in the distribution of PS1 immunoreactivity or in the distribution of PS1 molecules showing the strongest NT–CT FRET between the wild-type PS1- and M146L PS1-expressing neurons (Fig. 4), although the strongest FRET value (FITC lifetime shortening) was different for wild-type and M146L mutant PS1 neurons. Although the absolute values of the FITC lifetime slightly differ in different preparations, the direction of the change for wild-type PS1 and FAD PS1 mutants is identical among CHO cells, N2a cells, and primary neurons.

Effects of NSAIDs on PS1 NT–CT interactions

Our recent data suggest that NSAIDs affect the proximity of the NT to the CT of PS1 in a way as to decrease the amount of FRET observed between the two sites (Lleo et al., 2004b). We interpreted this effect to suggest an allosteric interaction with PS1/γ-secretase, leading to a conformation change of PS1. The effect of NSAIDs (which selectively lower $A\beta_{42}$ and enhance $A\beta_{38}$ production) is the opposite of that observed herein for the effects of FAD-linked PS1 mutations, which increase $A\beta_{42}$. We treated neurons expressing wild-type or M146L PS1 with ibuprofen, indomethacin, or vehicle (EtOH) and measured PS1 NT–CT proximity. In both the wild-type and M146L neurons, treatment with either ibuprofen or indomethacin increased the fluorescence lifetimes (Table 4), consistent with our previous observations that these drugs alter the PS1/γ-secretase conformation in a way as to diminish PS1 NT–CT proximity (Lleo et al., 2004b).

Effect of PS1 FAD mutations on APP–PS1 interactions

Because FAD mutations in PS1 lead to a shift in the site preference of APP γ-secretase cleavage from the $A\beta_{40}$ to the $A\beta_{42}$ position, we postulated that alterations in PS1 conformation might lead to a difference in APP–PS1 spatial interactions. We used a FLIM assay of APP–PS1 interactions we recently developed based on the proximity of the APP CT and PS1 loop domains (Berezovska et al., 2003) to determine whether the PS1 mutations affected this interaction. In this assay, a change in the FITC lifetime represents the change in the distance between the PS1 loop and APP–CT in cells expressing FAD mutant PS1 compared with that in wild-type PS1-expressing cells. Change in the relative proximity of these epitopes would reflect an alteration of the structure of the PS1–APP complex and thus be consistent with a model in which FAD mutants alter how APP substrate is presented to the active site of γ-secretase. We found that the six FAD PS1 mutations tested (Δex9 mutation lacks the loop epitope) displayed a decreased measured fluorescence lifetime, reflecting an increase in the proximity of the PS1 loop to the APP CT compared with wild-type PS1 (Table 5). This result is consistent with the hypothesis that FAD-linked mutations in PS1 lead to a common alteration in the proximity between the PS1 NT and CT, which then leads to a change in the alignment of PS1 and APP, potentially accounting for the shift in the Aβ cleavage site between positions 40 and 42. As expected, the nonpathogenic E318G PS1 polymorphism did not significantly change the posi-

tioning of the PS1 loop domain relative to the APP CT as reflected by unaltered FITC fluorescence lifetime (Table 5) compared with that of wild-type PS1.

Discussion

Our goal was to assess the effect of FAD PS1 mutations, using an assay that we recently developed that reflects the conformational state of PS1 in intact cells (Lleo et al., 2004b). By labeling different domains of a complex multipass transmembrane protein, PS1, we were able to study the relative proximity of those domains to one another *in situ*. The assay uses a highly sensitive FLIM technique to detect comparative changes in the positioning of one domain (or one molecule) relative to another domain of the same molecule (or another molecule) within intact cells and therefore provides an indirect assessment of the conformation of the protein or complex.

We empirically examined multiple different pairs of epitopes on PS1. We found two populations of donor fluorophore lifetimes in cells immunostained with antibodies against the PS1 NT and CT: non-FRETing with the PS1 NT far apart from the PS1 CT, which we interpret to be immature PS1 holoprotein, and a FRETing population with the NT–CT distance <10 nm, which we interpret to be functionally active PS1. The FLIM assay allows direct visualization of the subcellular distribution of these two PS1 populations: the immature protein, which is observed in the perinuclear area [in the endoplasmic reticulum (ER)], and the mature complex, which is present primarily in more distal cell compartments and near the cell surface (Fig. 1). This is consistent with the observation that active PS1 containing γ-secretase complex interacts with substrate at or near the cell surface (Ray et al., 1999; Berezovska et al., 2003; Ramdya et al., 2003). In contrast, we did not detect any FRET between the NT and CT in inactive or immature PS1 holoprotein, either because the heterodimeric cleavage did not occur and/or because the detected NT and CT conformation depends on additional interactions with other members of the γ-secretase complex. As expected, these data indicate that immature PS1 holoprotein and functionally active PS1 heterodimer are in different conformational states. Our data add to this general concept by indicating that they differ (at least in part) by a specific spatial relationship between the PS1 NT and CT.

The most straightforward explanation for these data would be the generation of a ring structure in which the PS1 NT and CT come close together when in active form, which is in agreement with a model proposed based on serial deletions and coimmunoprecipitation experiments (Annaert et al., 2001; Esler et al., 2002). An alternative explanation of the presence or absence of FRET between the PS1 NT and CT could be the formation of PS1 dimers (multimers) in the course of functional maturation of the PS1/γ-secretase complex. In favor of this hypothesis, cross-linking and coimmunoprecipitation experiments suggest the presence of PS1 NT fragment homodimers in active γ-secretase (Schroeter et al., 2003). In addition, the presence of PS1 holoprotein homodimers was suggested by a recent finding, using a yeast two-hybrid system, of the ability of PS1 to self-associate and form specific full-length/full-length homodimers (Cervantes et al., 2001, 2004; Hebert et al., 2003). Our current data suggest that the NT and CT of PS1 heterodimers come into close proximity but do not distinguish whether this is because of a PS1 single molecule ring structure or a PS1 multimer formation, and both remain plausible models.

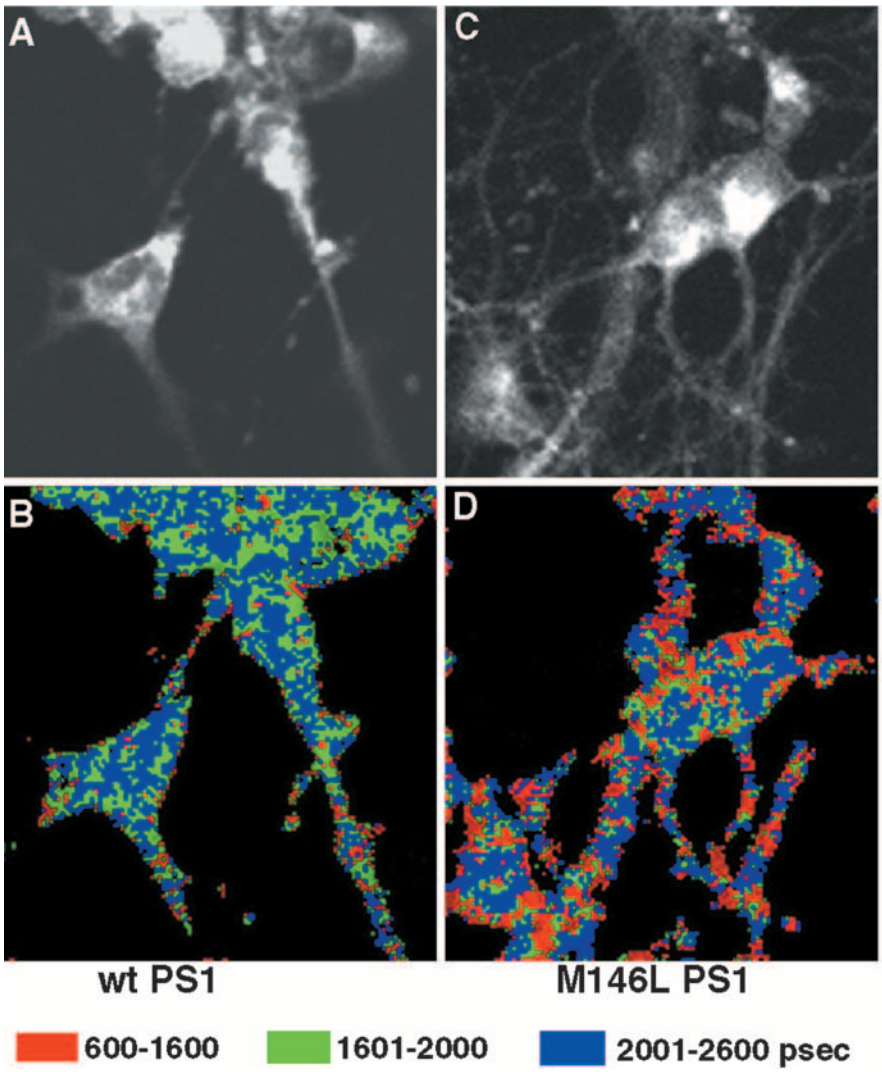

Figure 4. FLIM analysis of the PS1 NT–CT proximity in primary neurons expressing wild-type (wt) PS1 (***A***, ***B***) and M146L PS1 (***C***, ***D***). ***A***, ***C***, Intensity images of the FITC–PS1 immunoreactivity (x81 antibody). ***B***, ***D***, Pseudocolored FLIM images of the FITC lifetime distribution within neuronal cells. The FITC lifetimes are shown using discrete color-coding: red, 600–1600 picoseconds (psec); green, 1601–2000 psec; blue, 2001–2600 psec. Lifetimes significantly shorter than 2000 psec represent FRETing molecules with the PS1 NT and CT in close proximity.

Table 4. Effect of NSAIDs on wild-type or M146L PS1 transgenic neurons

	Alexa488 lifetime (*t2*; mean ± SD; ps)		
Condition	Vehicle	Ibuprofen	Indomethacin
PS1 wild type	2093 ± 41	2187 ± 42 ($p < 0.01$)	2157 ± 76 ($p < 0.01$)
PS1 M146L	1903 ± 96	2007 ± 74 ($p < 0.001$)	2014 ± 75 ($p < 0.001$)

p values are compared with vehicle (treatment with 0.3% EtOH). Alexa488–IgG lifetime in the absence of FRET was 2346 ± 37 ps. $n = 8–13$ cells per condition (ANOVA with Fisher's PLSD *post hoc* analysis). Similar results were observed in two replicate experiments.

Table 5. Effect of PS1 FAD mutations on the proximity between the APP CT and PS1 loop domain

Condition	FITC lifetime ($t2$; mean ± SD; ps)	p value (compared with wild-type PS1)
PS1 wild type ($n = 120$)	1872 ± 306	–
PS1 M139V ($n = 12$)	1520 ± 206	<0.01
PS1 M146L ($n = 40$)	1725 ± 370	<0.05
PS1 L166P ($n = 14$)	1586 ± 158	<0.04
PS1 L246V ($n = 40$)	1645 ± 393	<0.001
PS1 G384A ($n = 11$)	1641 ± 329	<0.05
PS1 C410Y ($n = 45$)	1427 ± 365	<0.001
PS1 E318G ($n = 15$)	1973 ± 361	ns

CHO cells were transiently transfected with either wild-type PS1 or FAD mutant PS1. FITC–IgG lifetime in the absence of FRET was 2347 ± 35 ps ($n = 96$). n, Cell number (ANOVA).

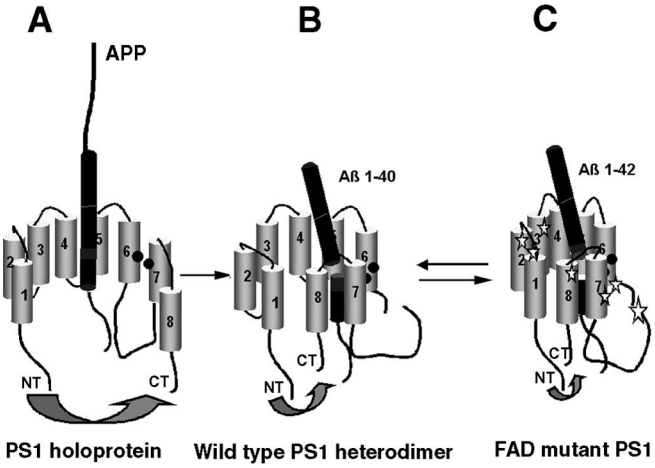

Figure 5. Schematic representation of the predicted PS1 conformation for immature PS1 holoprotein (***A***) and functionally active PS1 heterodimer complexes (***B***, ***C***). We postulate two closely related conformations, which may exist in a dynamic equilibrium. In this model, FAD mutations in PS1 shift the equilibrium to favor the conformation shown in ***C*** and stabilize the alignment of the active site of PS1/γ-secretase with the APP substrate to favor cleavage at $A\beta_{42}$ position on APP. The black circles in TM6 and TM7 indicate the position of aspartate 257 and aspartate 385, respectively (a putative catalytic site). The stars in ***C*** indicate the position of analyzed FAD PS1 mutations (small star, M139V, M146L, L166P, L286V, G384A, and C410Y; large star, exon 9 deletion). APP C99 substrate is aligned with PS1 to be predominantly cleaved at the $A\beta_{40}$ (***B***) or $A\beta_{42}$ (***C***) position. For simplicity, we show only one component of the multimeric γ-secretase complex and PS1 as a monomer, but analogous models with PS1 as a dimer or multimer are also possible.

Our observations regarding the conformation of the PS1 Δex9 mutants are particularly interesting. PS1 is known to require proteolytic cleavage within exon 9 to have catalytic activity. Paradoxically, a FAD-linked PS1 mutation that leads to the deletion of exon 9 prevents endoproteolysis of PS1, yet yields functionally active PS1 and results in increased $A\beta_{42}$ generation (Perez-Tur et al., 1995; Borchelt et al., 1996; Steiner et al., 2001). Our data help resolve this paradox by demonstrating that the mutant Δex9 PS1 can adopt a conformation similar to heterodimeric PS1 rather than to PS1 holoprotein. Indeed, the aberrant splicing leading to a deletion of exon 9 in PS1 introduces the point mutation, S290C, which contributes to the pathological activity (increased $A\beta_{42}$) similar to other missense PS1 mutations (Steiner et al., 1999). We interpret the FLIM results to suggest that the critical determinant in PS1 activity is achieving a specific protein conformation (represented by a close NT–CT interaction) rather than endoproteolysis per se.

Numerous FAD mutations in PS1 have been identified since the discovery of the PS1 gene (Sherrington et al., 1995) (www.alzforum.org). Although it is known that virtually all PS1 mutations cause a change in APP processing with increased production of the longer, highly fibrillogenic form of Aβ, it remains unclear how missense mutations scattered throughout the entire molecule and even a large deletion (Δexon 9) mutation that (uniquely) precludes cleavage of the holoprotein all lead to the same clinical phenotype. We hypothesized that a change in PS1 conformation and/or its subcellular distribution could be responsible for the effects on APP processing.

Our results demonstrate that all FAD mutations tested (both missense and deletion) located in the N-terminal domain, midregions, or C-terminal domain of the PS1 molecule did not significantly affect the subcellular distribution of the functionally active PS1 but lead to a consistent change in PS1 NT–CT proximity: bringing the epitopes closer together. We also found that the FAD-associated change in PS1 conformation leads to an alteration of the structure of the PS1–APP complex and affects how APP substrate is presented to the active site of γ-secretase. Overexpression of the nonpathogenic E318G polymorphism did not have these effects. Because each of the FAD-associated mutations also increases $A\beta_{42}$, we hypothesize that the change in conformation of PS1 and alteration in PS1–APP interactions leads to the biochemical phenotype of elevated $A\beta_{42}$ (Selkoe, 1998; Lleo et al., 2004a) and neuropathological phenotype of increased plaque deposition (Gomez-Isla et al., 1999) (i.e., that the change in conformation of PS1 we observe for multiple PS1 mutations represents a common molecular explanation for the AD-causing phenotype of PS1 mutations).

Our recent data show that the $A\beta_{42}$-lowering NSAIDs have the opposite effect on PS1 NT–CT proximity (diminishing it) and on APP CT–PS1 interactions, further supporting a link between the PS1 epitope conformation we examine and the $A\beta_{42}$-generating activity of γ-secretase (Lleo et al., 2004b). Treatment of mutant M146L-expressing neurons with two nonsteroidal medications reduced the effect of the mutation on PS1 NT–CT conformation, suggesting a direct approach toward diminishing the effect of the mutation on PS1. It is important to note, however, that the doses used in these model systems are substantially higher than the doses given to humans.

Although the strength of the FRET technique we present here is that it reports proximity of molecules or subdomains of molecules within an intact cellular environment, there are several limitations. Differences in subcellular localization of different conformational species are somewhat qualitative, and certainly subtle differences could be overlooked. Moreover, the current studies of mutant PS1 were performed in overexpressing cells, or in neurons of transgenic mice overexpressing PS1 or mutant PS1, and it is possible that trafficking of PS1 under these conditions may differ from that of PS1 present at endogenous levels. However, both stably transfected CHO and primary neurons were used, with consistent results. Importantly, overexpression of the non-FAD-associated E318G polymorphism revealed FRET data similar to wild-type PS1, whereas all six different FAD-associated mutations led to a consistent shortening of the donor fluorophore lifetimes.

Based on these data, we propose a model in which immature PS1 is initially present in an inactive conformation represented by long (>10 nm) distance between its N and C termini (Fig. 5*A*). Because the PS1 molecule traffics through subcellular compartments, matures, and associates with other members of the γ-secretase complex, we propose that it adopts an active conformation in which the NT–CT of PS1 molecules come close together. The effects of the FAD-associated mutations that we study

here, combined with our recent observations of a change in PS1 NT–CT proximity as a result of presumed allosteric interactions of nonsteroidal agents (Lleo et al., 2004b), lead us to propose an additional refinement to this model. We propose that the subpopulation of catalytically active PS1 molecules may reflect a mixture of meta-stable conformations with the NT and CT domains either somewhat closer together or somewhat further apart, corresponding to changes in PS1–APP interactions and accounting for γ-cleavage at $A\beta_{42}$ and $A\beta_{40,}$ respectively (Fig. 5*B*,*C*). We propose that FAD PS1 mutations change the molecular kinetics to favor the second conformational state (NT–CT closer together) (Fig. 5*C*) and therefore lead to an increase in the $A\beta_{42}/A\beta_{40}$ ratio. In accordance with this model, the nonsteroidal drugs that lower $A\beta_{42}$ have the opposite effect on PS1 NT–CT proximity (Weggen et al., 2001; Lleo et al., 2004b) .

Understanding such a change in PS1 conformation may contribute to rational drug design strategies, allowing the design of compounds that act allosterically to stabilize the more "open" active conformation, in contrast to inhibiting the proteolytic activity of the γ-secretase (Lleo et al., 2004b). More generally, the approach we highlight here using FLIM allows detection of relative changes in protein conformation in intact and/or living cells without disrupting the normal physiological environment of the protein. This may be especially useful for studying protein–protein interactions *in situ* in specific subcellular compartments in intact cell preparations.

References

Aldudo J, Bullido MJ, Frank A, Valdivieso F (1998) Missense mutation E318G of the presenilin-1 gene appears to be a nonpathogenic polymorphism. Ann Neurol 44:985–986.

Annaert WG, Esselens C, Baert V, Boeve C, Snellings G, Cupers P, Craessaerts K, De Strooper B (2001) Interaction with telencephalin and the amyloid precursor protein predicts a ring structure for presenilins. Neuron 32:579–589.

Bacskai BJ, Skoch J, Hickey GA, Allen R, Hyman BT (2003) FRET determinations using multiphoton fluorescence lifetime imaging microscopy (FLIM) to characterize amyloid-beta plaques. J Biomed Opt 8:368–375.

Berezovska O, Frosch M, McLean P, Knowles R, Koo E, Kang D, Shen J, Lu FM, Lux SE, Tonegawa S, Hyman BT (1999) The Alzheimer-related gene presenilin 1 facilitates notch 1 in primary mammalian neurons. Brain Res Mol Brain Res 69:273–280.

Berezovska O, Jack C, McLean P, Aster JC, Hicks C, Xia W, Wolfe MS, Kimberly WT, Weinmaster G, Selkoe DJ, Hyman BT (2000) Aspartate mutations in presenilin and gamma-secretase inhibitors both impair notch1 proteolysis and nuclear translocation with relative preservation of notch1 signaling. J Neurochem 75:583–593.

Berezovska O, Ramdya P, Wolfe MS, Bacskai BJ, Hyman BT (2003) APP associates with a nicastrin depending docking site on the PS1/γ-secretase complex in cells demonstrated by fluorescence lifetime imaging. J Neurosci 23:4560–4566.

Borchelt D, Thinakaran G, Eckman C, Lee M, Davenport F, Ratovitsky T, Prada C, Kim G, Seekins S, Yager D, Slunt H, Wang R, Seeger M, Levey A, Gandy S, Copeland N, Jenkins N, Price D, Younkin S, Sisodia S (1996) Familial Alzheimer's disease-linked presenilin 1 variants elevate Aβ1–42/1–40 ratio in vitro and in vivo. Neuron 17:1005–1013.

Capell A, Grunberg J, Pesold B, Diehlmann A, Citron M, Nixon R, Beyreuther K, Selkoe DJ, Haass C (1998) The proteolytic fragments of the Alzheimer's disease-associated presenilin-1 form heterodimers and occur as a 100–150-kDa molecular mass complex. J Biol Chem 273:3205–3211.

Cervantes S, Gonzalez-Duarte R, Marfany G (2001) Homodimerization of presenilin N-terminal fragments is affected by mutations linked to Alzheimer's disease. FEBS Lett 505:81–86.

Cervantes S, Saura CA, Pomares E, Gonzalez-Duarte R, Marfany G (2004) Functional implications of the presenilin dimerization: reconstitution of gamma-secretase activity by assembly of a catalytic site at the dimer interface of two catalytically inactive presenilins. J Biol Chem 279:36519–36529.

De Strooper B, Annaert W, Cupers P, Saftig P, Craessaerts K, Mumm JS, Schroeter EH, Schrijvers V, Wolfe MS, Ray WJ, Goate A, Kopan R (1999) A presenilin-1-dependent gamma-secretase-like protease mediates release of Notch intracellular domain. Nature 398:518–522.

Doan A, Thinakaran G, Borchelt DR, Slunt HH, Ratovitsky T, Podlisny M, Selkoe DJ, Seeger M, Gandy SE, Price DL, Sisodia SS (1996) Protein topology of presenilin 1. Neuron 17:1023–1030.

Edbauer D, Winkler E, Haass C, Steiner H (2002) Presenilin and nicastrin regulate each other and determine amyloid beta-peptide production via complex formation. Proc Natl Acad Sci USA 99:8666–8671.

Esler WP, Kimberly WT, Ostaszewski BL, Ye W, Diehl TS, Selkoe DJ, Wolfe MS (2002) Activity-dependent isolation of the presenilin-gamma-secretase complex reveals nicastrin and a gamma substrate. Proc Natl Acad Sci USA 99:2720–2725.

Fortini ME (2002) Gamma-secretase-mediated proteolysis in cell-surface-receptor signalling. Nat Rev Mol Cell Biol 3:673–684.

Francis R, McGrath G, Zhang J, Ruddy DA, Sym M, Apfeld J, Nicoll M, Maxwell M, Hai B, Ellis MC, Parks AL, Xu W, Li J, Gurney M, Myers RL, Himes CS, Hiebsch R, Ruble C, Nye JS, Curtis D (2002) aph-1 and pen-2 are required for Notch pathway signaling, gamma-secretase cleavage of betaAPP, and presenilin protein accumulation. Dev Cell 3:85–97.

Fraser PE, Yang D, Yu G, Levesque L, Nishimura M, Arawaka S, Serpell L, Rogaeva E, George-Hyslop PS (2000) Presenilin structure, function and role in Alzheimer disease. Biochem Biophys Acta 1502:1–15.

Gomez-Isla T, Growdon WB, McNamara MJ, Nochlin D, Bird TD, Arango JC, Lopera F, Kosik KS, Lantos PL, Cairns NJ, Hyman BT (1999) The impact of different presenilin 1 and presenilin 2 mutations on amyloid deposition, neurofibrillary changes and neuronal loss in the familial Alzheimer's disease brain: evidence for other phenotype-modifying factors. Brain 122:1709–1719.

Goutte C, Tsunozaki M, Hale VA, Priess JR (2002) APH-1 is a multipass membrane protein essential for the Notch signaling pathway in *Caenorhabditis elegans* embryos. Proc Natl Acad Sci USA 99:775–779.

Hebert S, Godin C, Tomiyama T, Mori H, Levesque G (2003) Dimerization of presenilin-1 in vivo: suggestion of novel regulatory mechanisms leading to higher order complexes. Biochem Biophys Res Commun 301:119–126.

Kowalska A, Wender M, Florczak J, Pruchnik-Wolinska D, Modestowicz R, Szczech J, Rossa G, Kozubski W (2003) Molecular genetics of Alzheimer's disease: presenilin 1 gene analysis in a cohort of patients from the Poznan region. J Appl Genet 44:231–234.

Levitan D, Lee J, Song L, Manning R, Wong G, Parker E, Zhang L (2001) PS1 N- and C-terminal fragments form a complex that functions in APP processing and Notch signaling. Proc Natl Acad Sci USA 98:12186–12190.

Li X, Greenwald I (1996) Membrane topology of the *C. elegans* SEL-12 presenilin. Neuron 17:1015–1021.

Li X, Greenwald I (1998) Additional evidence for an eight-transmembrane-domain topology for *Caenorhabditis elegans* and human presenilins. Proc Natl Acad Sci USA 95:7109–7114.

Lleo A, Berezovska O, Growdon JH, Hyman BT (2004a) Clinical, pathological, and biochemical spectrum of Alzheimer disease associated with PS-1 mutations. Am J Geriatr Psychiatry 12:146–156.

Lleo A, Berezovska O, Herl L, Raju S, Deng A, Bacskai BJ, Frosch MP, Irizarry M, Hyman BT (2004b) Nonsteroidal anti-inflammatory drugs lower Abeta(42) and change presenilin 1 conformation. Nat Med 10:1065–1066.

Perez-Tur J, Froelich S, Prihar G, Crook R, Baker M, Duff K, Wragg M, Busfield F, Lendon C, Clark RF, Rogues P, Fuldner RA, Johnson J, Cowburn R, Forsell C, Axelman K, Lilius L, Houlden H, Karran E, Roberts GW, et al. (1995) A mutation in Alzheimer's disease destroying a splice acceptor site in the presenilin-1 gene. NeuroReport 7:297–301.

Podlisny MB, Citron M, Amarante P, Sherrington R, Xia W, Zhang J, Diehl T, Levesque G, Fraser P, Haass C, Koo EH, Seubert P, St George-Hyslop P, Teplow DB, Selkoe DJ (1997) Presenilin proteins undergo heterogeneous endoproteolysis between Thr291 and Ala299 and occur as stable N- and C-terminal fragments in normal and Alzheimer brain tissue. Neurobiol Dis 3:325–337.

Ramdya P, Skoch J, Bacskai BJ, Hyman BT, Berezovska O (2003) Activated Notch1 associates with a presenilin-1/gamma-secretase docking site. J Neurochem 87:843–850.

Ray WJ, Yao M, Mumm J, Schroeter EH, Saftig P, Wolfe M, Selkoe DJ, Kopan R, Goate AM (1999) Cell surface presenilin-1 participates in the

gamma-secretase-like proteolysis of Notch. J Biol Chem 274:36801–36807.

Scheuner D, Eckman C, Jensen M, Song X, Citron M, Suzuki N, Bird TD, Hardy J, Hutton M, Kukull WA, Larson E, Levy-Lahad E, Viitanen M, Peskind E, Poorkaj P, Schellenberg GD, Tanzi R, Wasco W, Lannfelt L, Selkoe D, et al. (1996) Secreted amyloid beta-protein similar to that in the senile plaques of Alzheimer's disease is increased in vivo by the presenilin 1 and 2 and APP mutations linked to familial Alzheimer's disease. Nat Med 2:864–870.

Schroeter EH, Ilagan MX, Brunkan AL, Hecimovic S, Li YM, Xu M, Lewis HD, Saxena MT, De Strooper B, Coonrod A, Tomita T, Iwatsubo T, Moore CL, Goate A, Wolfe MS, Shearman M, Kopan R (2003) A presenilin dimer at the core of the gamma-secretase enzyme: insights from parallel analysis of Notch 1 and APP proteolysis. Proc Natl Acad Sci USA 100:13075–13080.

Seeger M, Nordstedt C, Petanceska S, Kovacs DM, Gouras GK, Hahne S, Fraser P, Levesque L, Czernik AJ, George-Hyslop PS, Sisodia SS, Thinakaran G, Tanzi RE, Greengard P, Gandy S (1997) Evidence for phosphorylation and oligomeric assembly of presenilin 1. Proc Natl Acad Sci USA 94:5090–5094.

Selkoe D, Podlisny M, Joachim C, Vickers E, Lee G, Fritz L, Oltersdor T (1988) Beta-amyloid precursor protein of Alzheimer disease occurs as 110- to 135-kilodalton membrane-associated proteins in neural and nonneural tissues. Proc Natl Acad Sci USA 85:7341–7345.

Selkoe DJ (1998) The cell biology of beta-amyloid precursor protein and presenilin in Alzheimer's disease. Trends Cell Biol 8:447–453.

Selkoe DJ (2001) Presenilin, Notch, and the genesis and treatment of Alzheimer's disease. Proc Natl Acad Sci USA 98:11039–11041.

Sherrington R, Rogaev EI, Liang Y, Rogaeva EA, Levesque G, Ikeda M, Chi H, Lin C, Li G, Holman K, Tsuda T, Mar L, Foncin J-F, Bruni AC, Montesi MP, Sorbi S, Rainero I, Pinessi L, Nee L, Chumakov I, et al. (1995) Cloning of a gene bearing missense mutations in early-onset familial Alzheimer's disease. Nature 375:754–760.

Steiner H, Romig H, Grim M, Philipp U, Pesold B, Citron M, Baumeister R, Haass C (1999) The biological and pathological function of the presenilin-1 Deltaexon 9 mutation is independent of its defect to undergo proteolytic processing. J Biol Chem 274:7615–7618.

Steiner H, Revesz T, Neumann M, Romig H, Grim MG, Pesold B, Kretzschmar HA, Hardy J, Holton JL, Baumeister R, Houlden H, Haass C (2001) A pathogenic presenilin-1 deletion causes abberrant Abeta 42 production in the absence of congophilic amyloid plaques. J Biol Chem 276:7233–7239.

Thinakaran G, Borchelt DR, Lee MK, Slunt HH, Spitzer L, Kim G, Ratovitsky T, Davenport F, Nordstedt C, Seeger M, Hardy J, Levey AI, Gandy SE, Jenkins NA, Copeland NG, Price DL, Sisodia SS (1996) Endoproteolysis of presenilin 1 and accumulation of processed derivatives in vivo. Neuron 17:181–190.

Weggen S, Eriksen JL, Das P, Sagi SA, Wang R, Pietrzik CU, Findlay KA, Smith TE, Murphy MP, Bulter T, Kang DE, Marquez-Sterling N, Golde TE, Koo EH (2001) A subset of NSAIDs lower amyloidogenic Abeta42 independently of cyclooxygenase activity. Nature 414:212–216.

Wolfe MS, Xia W, Ostaszewski BL, Diehl TS, Kimberly WT, Selkoe DJ (1999) Two transmembrane aspartates in presenilin-1 required for presenilin endoproteolysis and gamma-secretase activity. Nature 398:513–517.

Yu G, Chen F, Levesque G, Nishimura M, Zhang DM, Levesque L, Rogaeva E, Xu D, Liang Y, Duthie M, St George-Hyslop PH, Fraser PE (1998) The presenilin 1 protein is a component of a high molecular weight intracellular complex that contains beta-catenin. J Biol Chem 273:16470–16475.

Yu G, Nishimura M, Arawaka S, Levitan D, Zhang L, Tandon A, Song YQ, Rogaeva E, Chen F, Kawarai T, Supala A, Levesque L, Yu H, Yang DS, Holmes E, Milman P, Liang Y, Zhang DM, Xu DH, Sato C, et al. (2000) Nicastrin modulates presenilin-mediated notch/glp-1 signal transduction and betaAPP processing. Nature 407:48–54.

Zekanowski C, Peplonska B, Styczynska M, Religa D, Pfeffer A, Czyzewski K, Gabryelewicz T, Szybinska A, Kijanowska-Haladyna B, Kotapka-Minc S, Luczywek E, Barczak A, Wasiak B, Chodakowska-Zebrowska M, Przekop I, Kuznicki J, Barcikowska M (2004) The E318G substitution in PSEN1 gene is not connected with Alzheimer's disease in a large Polish cohort. Neurosci Lett 357:167–170.